

## **Sulfurous Zeosils for Dehydra-Decyclization of Tetrahydrofuran to Renewable Butadiene**

Raisa Carmen Andeme Ela<sup>1,2</sup>, Jorge Barroso<sup>5</sup>, Gaurav Kumar<sup>1,2</sup>, Kaivalya Gawande<sup>4</sup>, Sophie A. Brauer<sup>1,2</sup>, Manish Shetty<sup>3</sup>, Xinyu Li<sup>1</sup>, Wei Fan<sup>4</sup>, Bess Vlasisavljevich<sup>5\*</sup>, Paul J. Dauenhauer<sup>1,2\*</sup>

<sup>1</sup> Department of Chemical Engineering and Materials Science, University of Minnesota, 421 Washington Avenue SE, Minneapolis, Minnesota 55455, USA

<sup>2</sup> Center for Sustainable Polymers, University of Minnesota, 207 Pleasant Street, SE, Minneapolis, MN, 55455, USA

<sup>3</sup> Artie McFerrin Department of Chemical Engineering, Texas A&M University, 400 Bizzell Street, College Station, Texas 77843, USA

<sup>4</sup> Department of Chemical Engineering, University of Massachusetts Amherst, 686 North Pleasant Street, Amherst, Massachusetts 01003, USA

<sup>5</sup> Department of Chemistry, University of South Dakota, Churchill-Haines 115, 414 E Clark St, Vermillion, SD, 57069

\*Corresponding authors: hauer@umn.edu; bess.vlasisavljevich@usd.edu

Number of pages: 31  
Number of figures: 23  
Number of Schemes: 2  
Number of tables: 7

### Table of Contents

S1. Experimental Methods

S2. Results and Discussion

## Section 1: Experimental Methods

Na-MFI synthesis, and B, P, S sites impregnation. To make Na Si-MFI, about 11.47 g of DI was added to a 20 ml centrifuge tube; a mixture of 1.23g TPABr and 9.55g 1.0 M NaOH solution was then added. Upon complete dissolution, about 2.75g of CAB-O-SIL M5 was added stepwise as the silica source, and the mixture was transferred to the autoclave. The mixture was crystallized in an oven at 423 K for 48 hours. Then, the sample was rinsed thoroughly with DI water for five minutes, then dried overnight at 373 K. Finally, the sample was calcined for 12 hours at 823 K at a ramping rate of 1 K/min. For B, P and S active site impregnation, targeting a theoretical ratio of  $\text{Si}/\text{X} = 27$  ( $\text{X} = \text{B}, \text{P}, \text{S}$ ), 0.72 wt % aqueous phosphoric acid solution ( $\text{H}_3\text{PO}_4$ ), 0.44 wt % aqueous boric acid solution ( $\text{H}_3\text{BO}_3$ ), and 0.69 wt % aqueous sulfuric acid solution ( $\text{H}_2\text{SO}_4$ ) were used. About 3.35 mL of the acidic solution were mixed with 0.4 g of calcined MFI and stirred on a magnetic stirrer at 300 RPM for five minutes. Then, the solution was dried at 70 °C under the static conditions, while covered with the aluminum foil. The dried powder was grinded and calcined at 600 °C for 30 minutes, with a 90-minute ramp to 600 °C under flowing air at 100 mL/min.

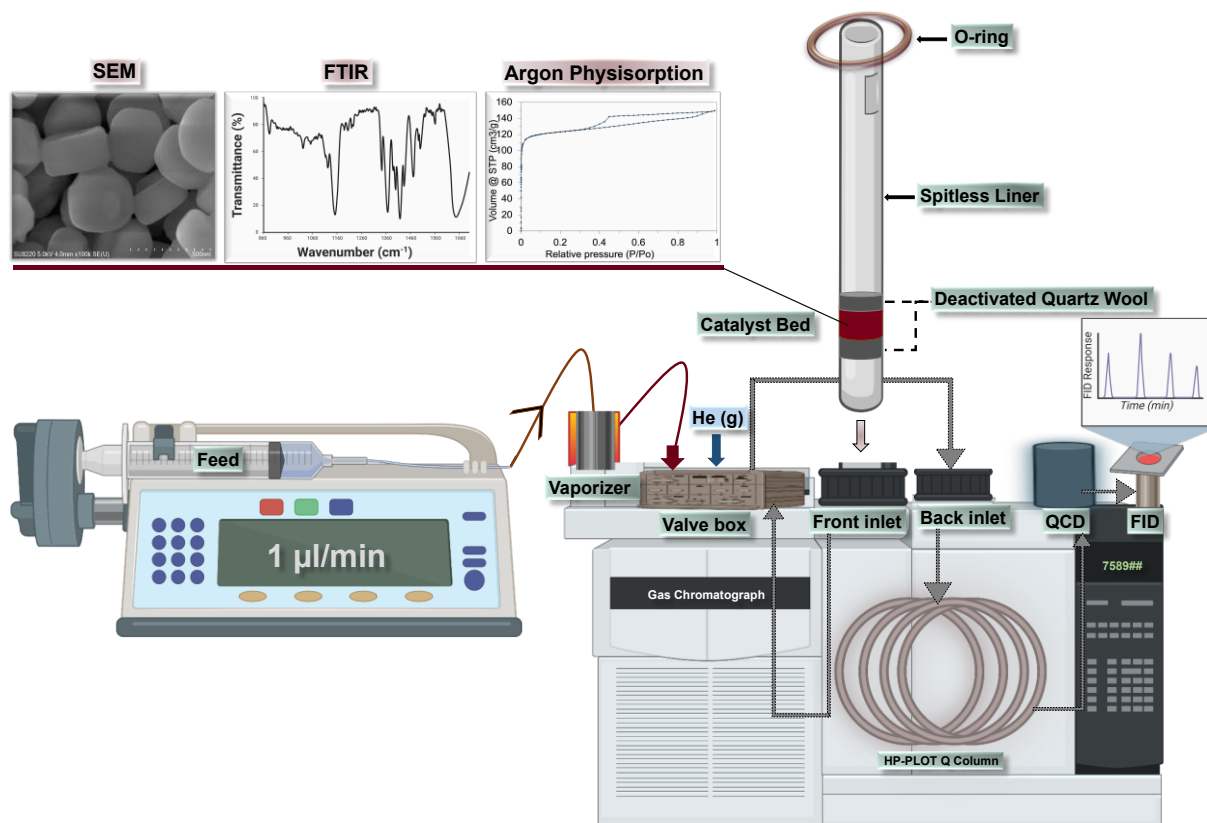


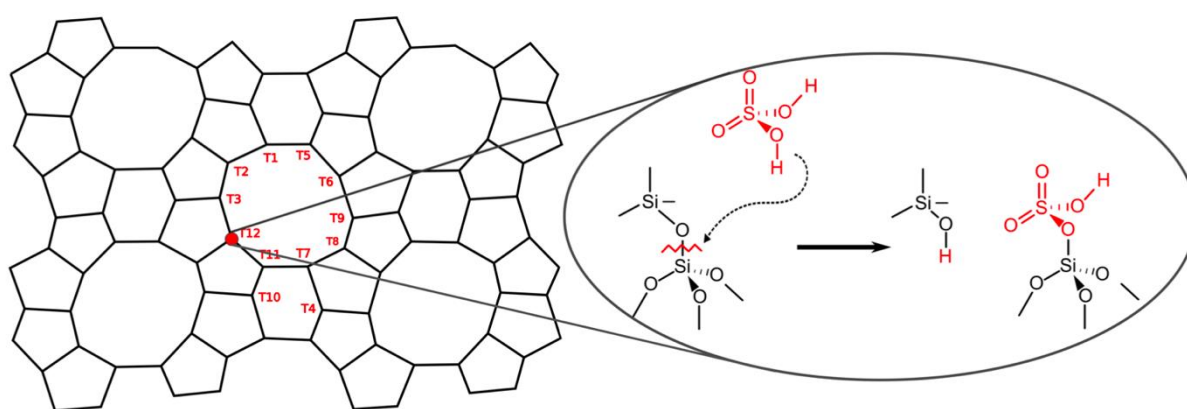
**Figure S1.** Schematic of micro-catalytic system utilized to conduct kinetic measurements for THF conversion over B, P, S-MFI and their sodium ion-containing versions, and sample catalyst characterization techniques employed. Part of this figure was created in *Bio-Render.com*

The Yield of 1,3-BD was calculated according to Equation S1 below.

$$Yield_{1,3-BD} = \frac{\text{mols}_{1,3-BD\text{formed}}}{\text{Total mols THF in feed stream}}$$

Equation S1

**Statistical design of experiment.** Box-Behnken design, and analyses were performed in Minitab®, to study P-MFI performance for three factors: temperature (200-370 °C), weight hourly space velocity (WHSV 1.9 - 19.1 g THF/g Catalyst h), and water content in feed (0 – 10 % v/v). Input variables were generated with one replicate, and three center points, for a total of 15 base runs for one model. To analyze the data, corresponding conversion and 1,3-BD selectivity values were input to the software, and a stepwise model at confidence interval ( $\alpha$ ) = 0.05 was generated. In Minitab®, Tukey's pairwise comparison of means was used to analyze and compare the performance of the six catalysts explored in this work at a confidence interval ( $\alpha$ ) = 0.05. This was also performed in Minitab®.



**Scheme S1.** Schematic representation of the T12 site, where the acid (sulfuric) is attached into the ZSM-5 structure.

## Section 2: Results and Discussion

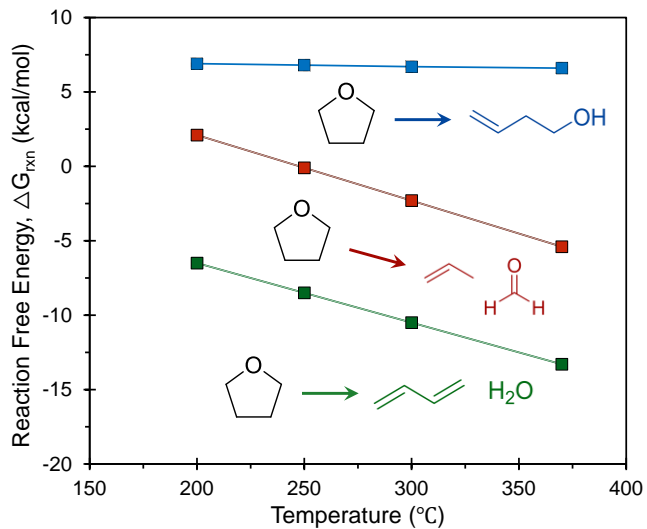


**Figure S2.** Vapor-phase thermochemistry of dehydro-decyclization of tetrahydrofuran to produce butadiene and water (highlighted in green), in competition with propene and formaldehyde (highlighted in red), and 3-butene-1-ol (highlighted in blue).

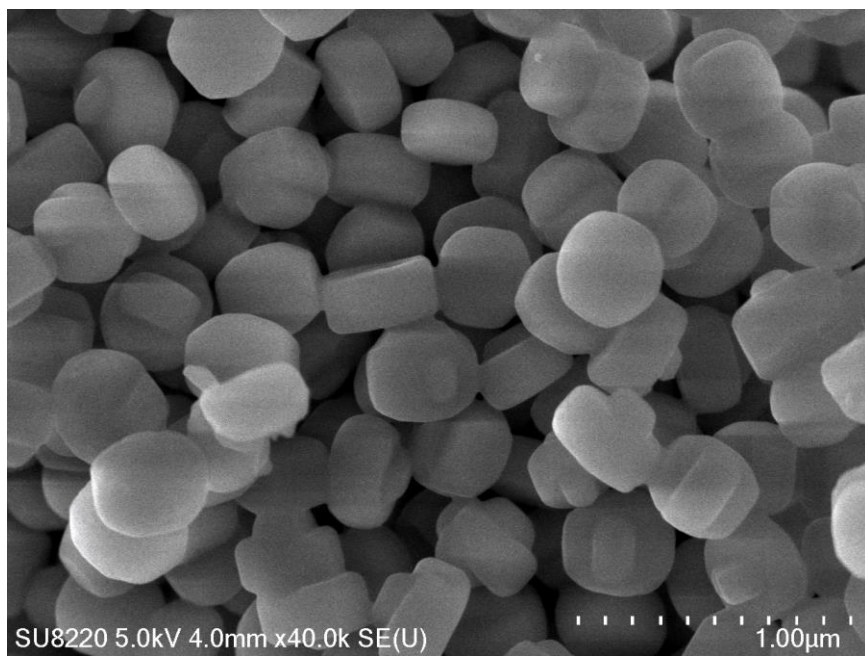


**Figure S3.** SEM micrograph of MFI crystallites before active site impregnation. The error bar represents a size of 1  $\mu\text{m}$ .

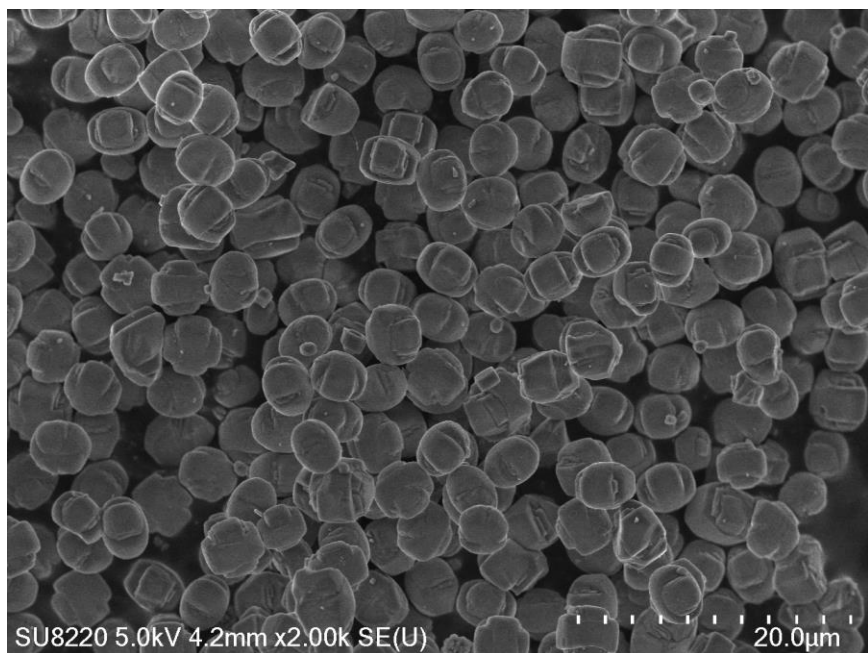


**Figure S4.** SEM micrograph of Na MFI crystallites before active site impregnation. The error bar represents a size of 20  $\mu\text{m}$ .

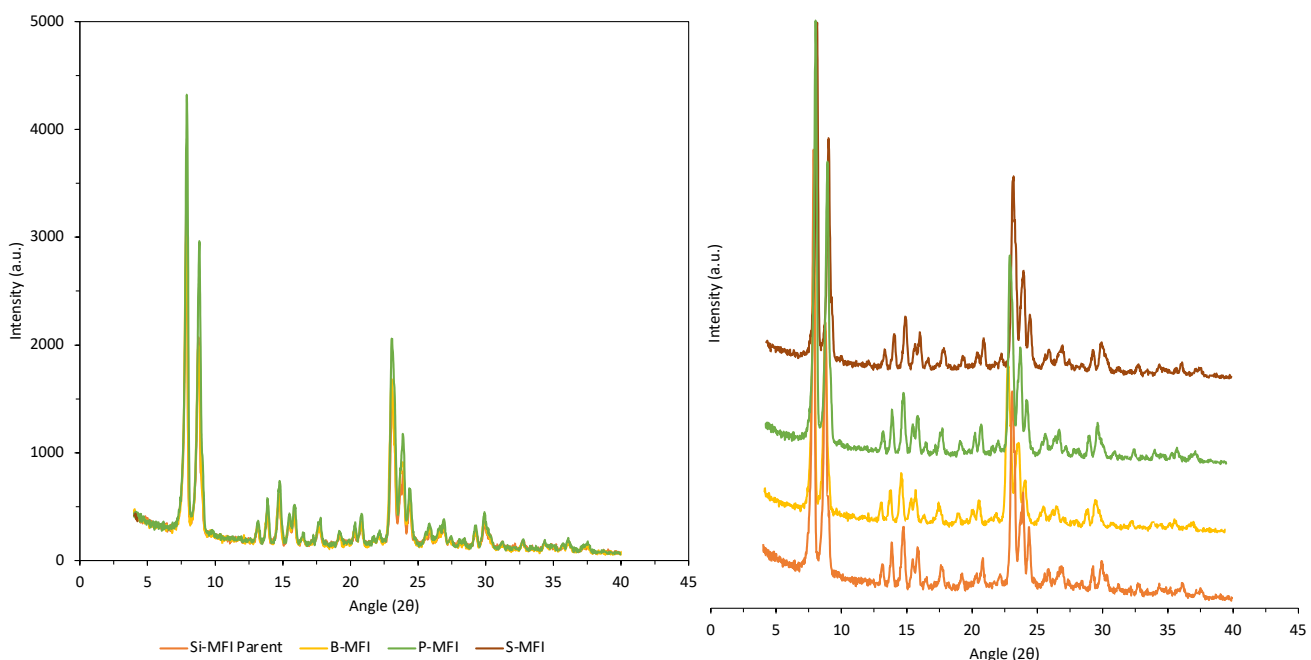


**Figure S5.** X-ray diffraction (XRD) graphs of MFI crystallites. Orange, pre-impregnated Si-MFI; yellow, B-MFI; green, P-MFI; brown, S-MFI.

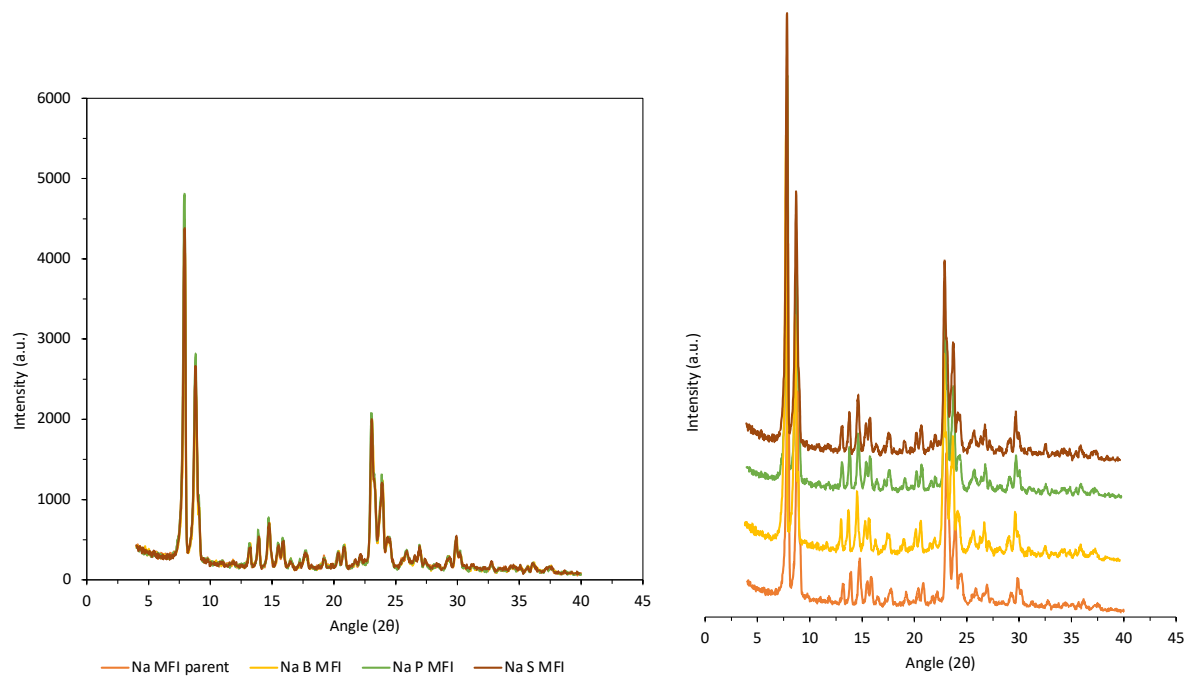


**Figure S6.** X-ray diffraction (XRD) graphs of Na MFI crystallites. Orange, pre-impregnated Na Si-MFI; yellow, Na B-MFI; green, Na P-MFI; brown, Na S-MFI.

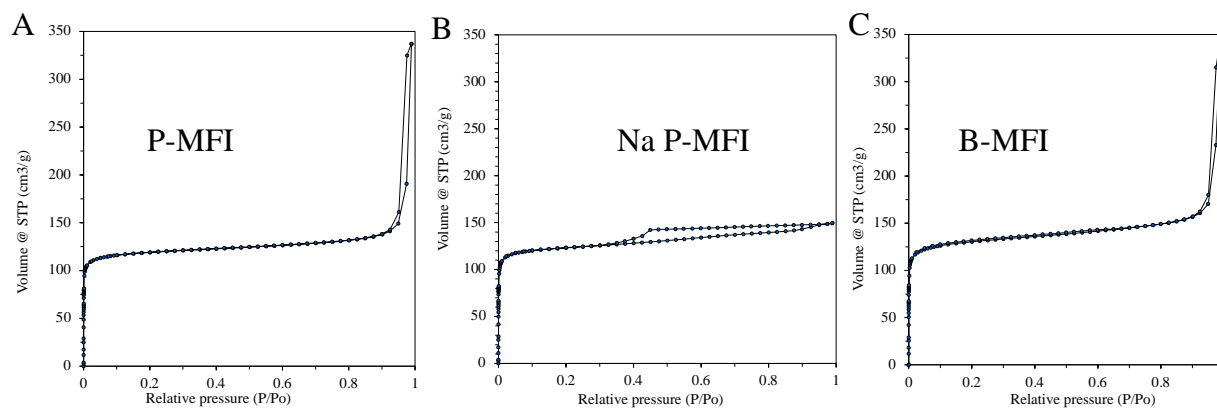


**Figure S7.** Representative argon (Ar) physisorption isotherms for **A** P-MFI, **B** Na P-MFI, and **C** B-MFI.



**Figure S8.** XPS elemental scan over the surface of B-MFI.

Sample\_3\_20220405\_101.spe

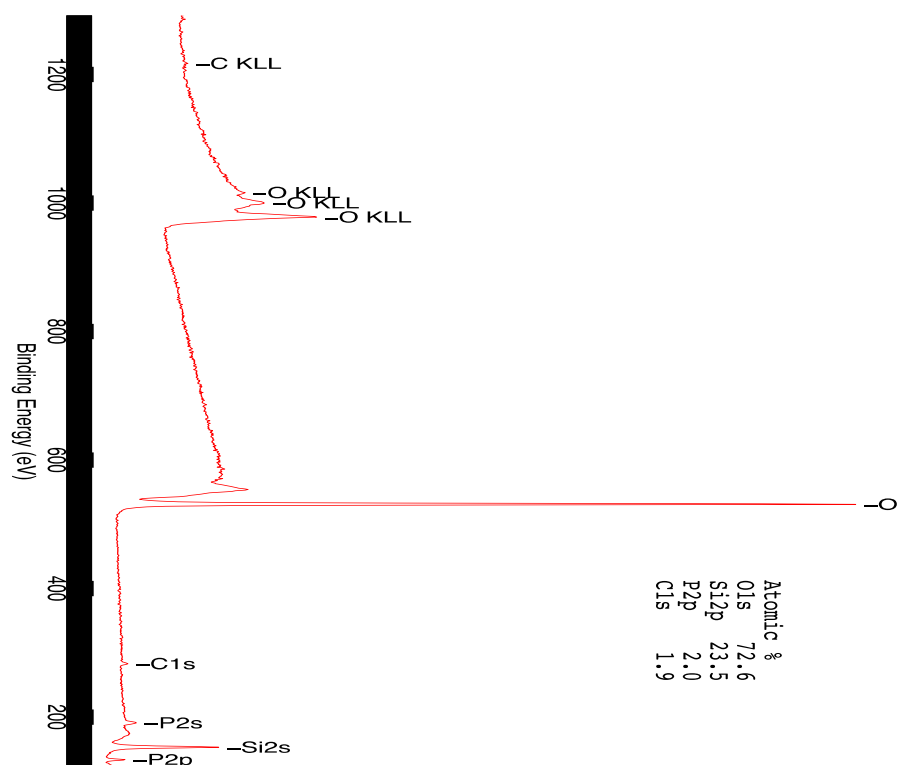


**Figure S9.** XPS elemental scan over the surface of P-MFI.

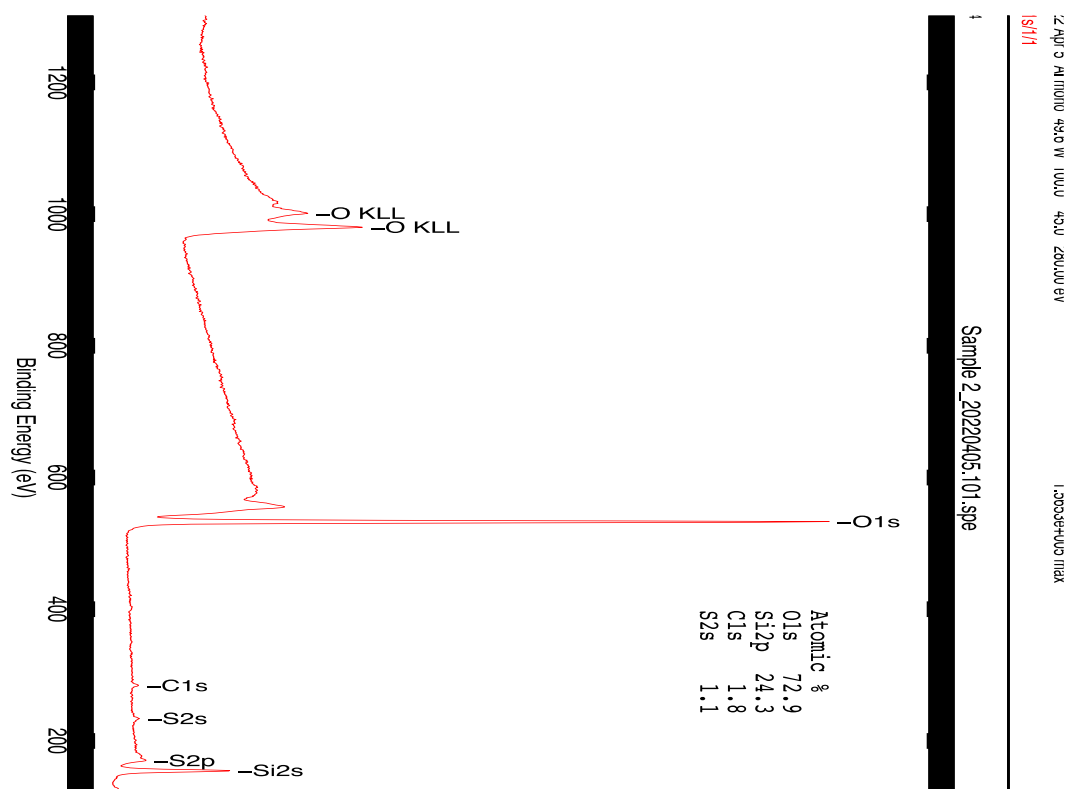


**Figure S10.** XPS elemental scan over the surface of S-MFI.

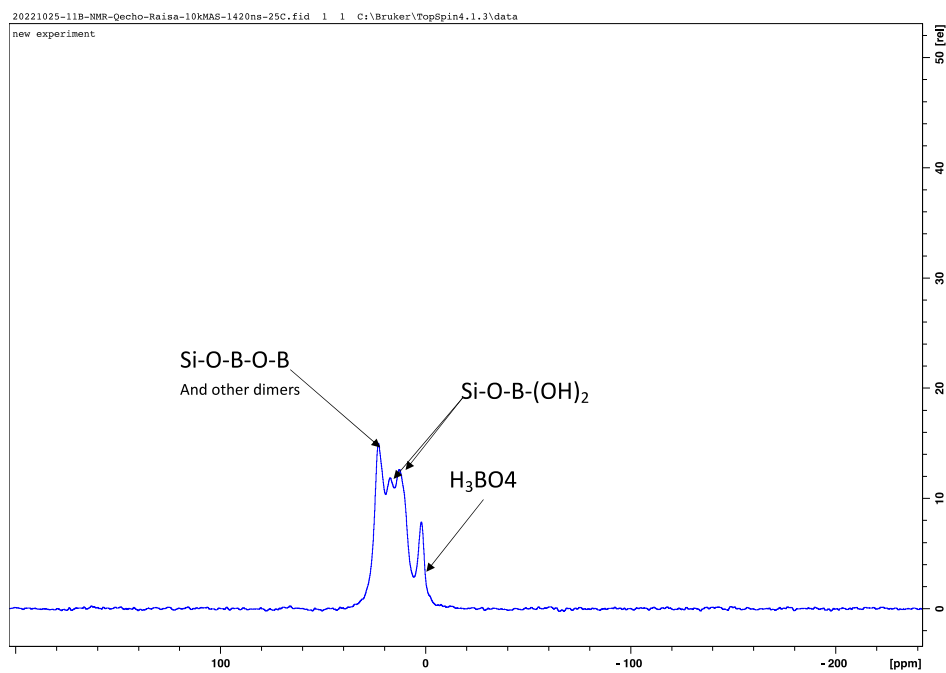


**Figure S11.** Solid State NMR of B-MFI. Plausible chemical structures.

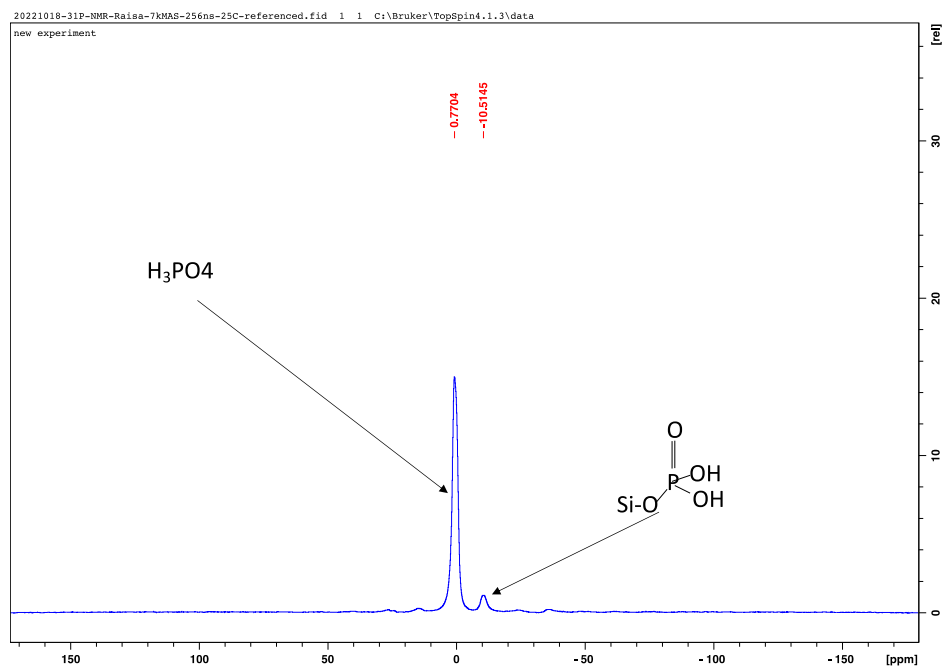


**Figure S12.** Solid State NMR of P-MFI. Plausible chemical structures.

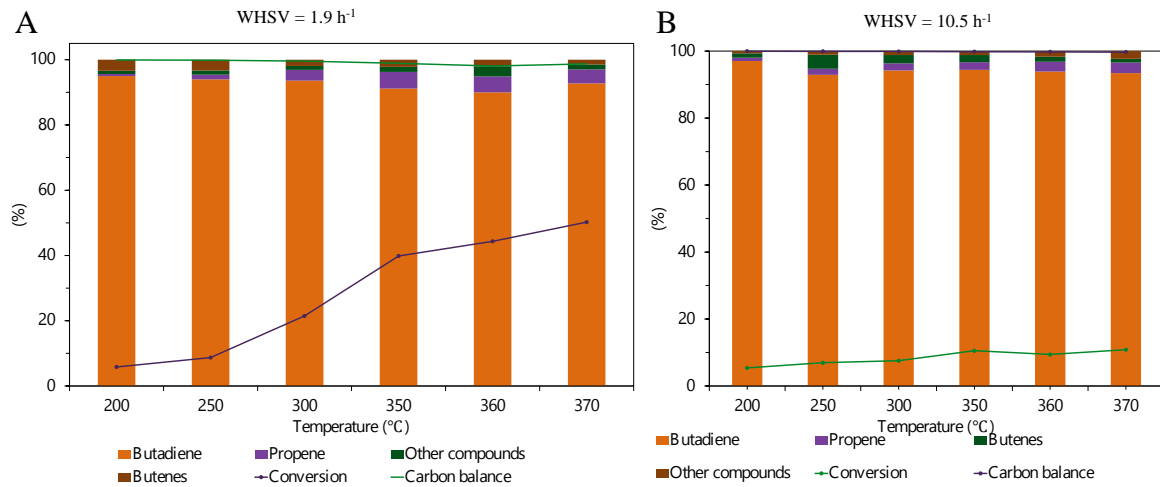


**Figure S13.** THF conversion and selectivity to BD performance over the P-MFI catalyst at A 1.9 and B 10.5 h<sup>-1</sup>. Carbon balances rounded off between 97.4 and 99.9 %. The error bars represent the standard deviation of at least three independent experimental replicates.

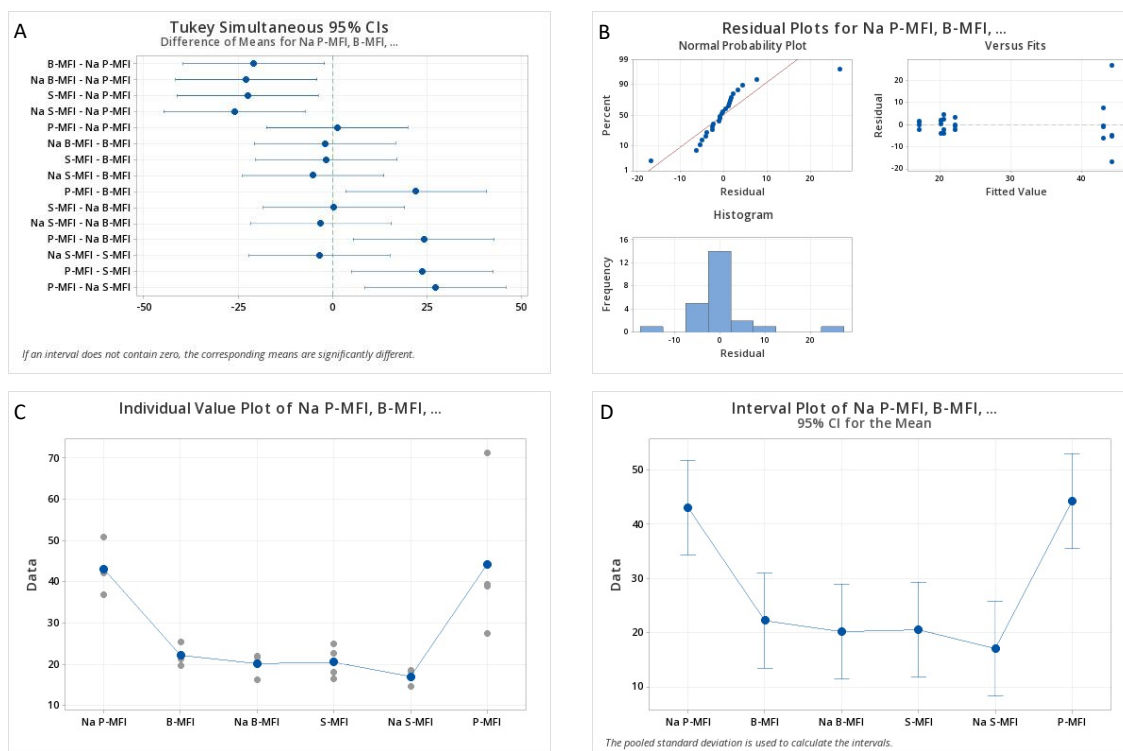


**Figure S14.** Residual, individual and interval plots for Tukey’s analysis of the conversion for all six catalysts.

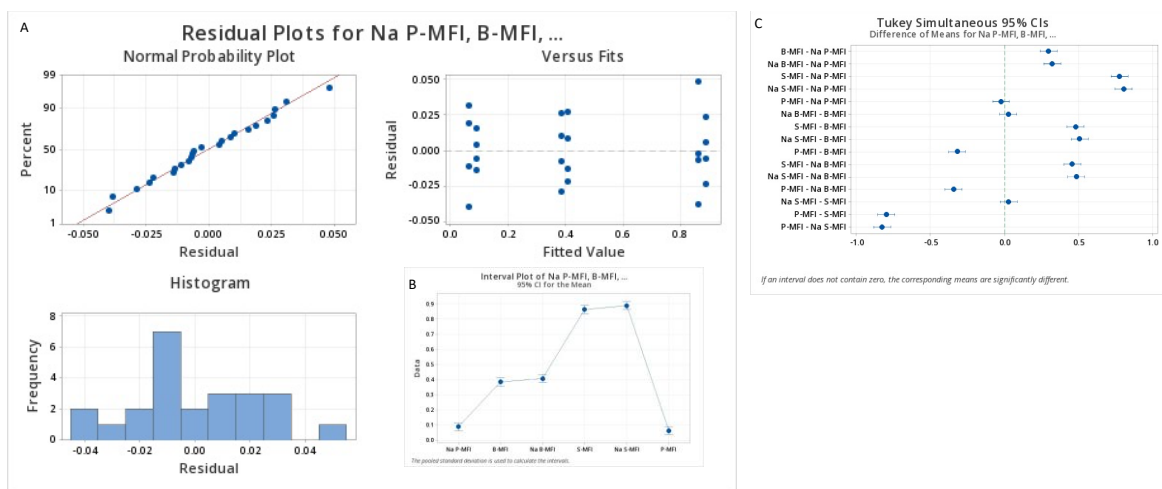


**Figure S15.** Residual, individual and interval plots for Tukey's analysis of the STYs for all six catalysts.

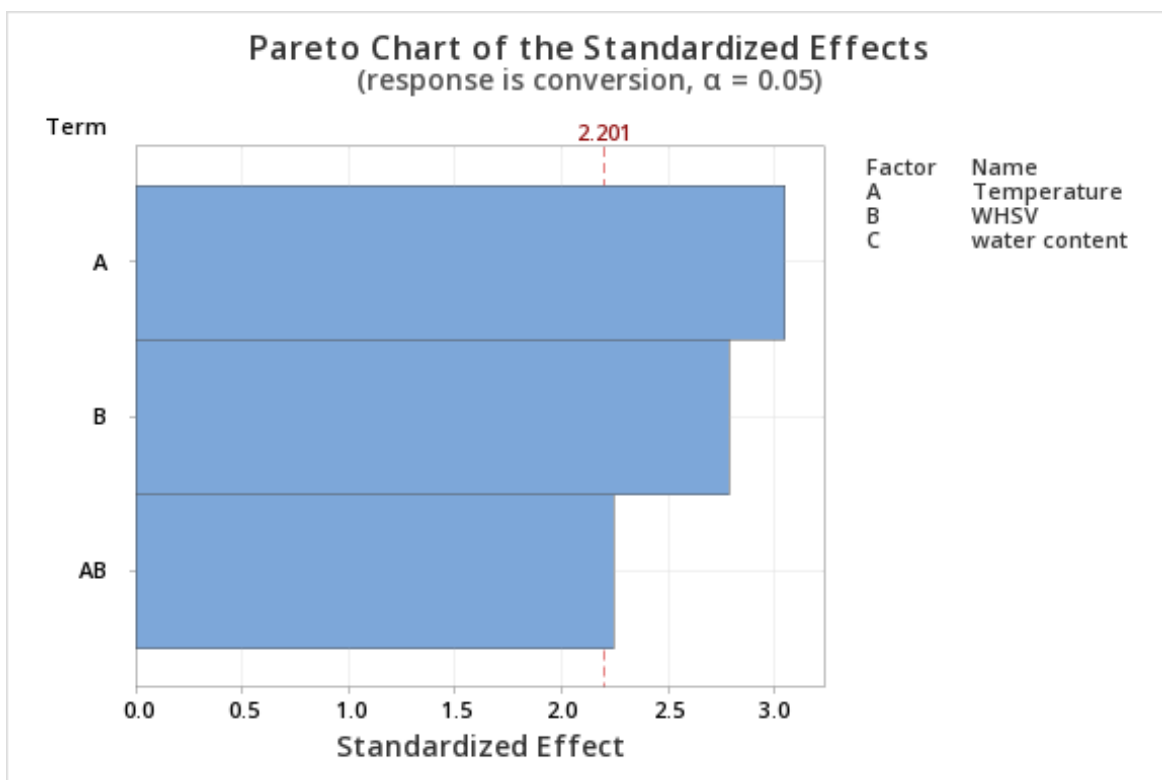


**Figure S16.** Pareto chart Box-Behnken model for conversion for factors that are statistically significant at a significance level of 0.05.

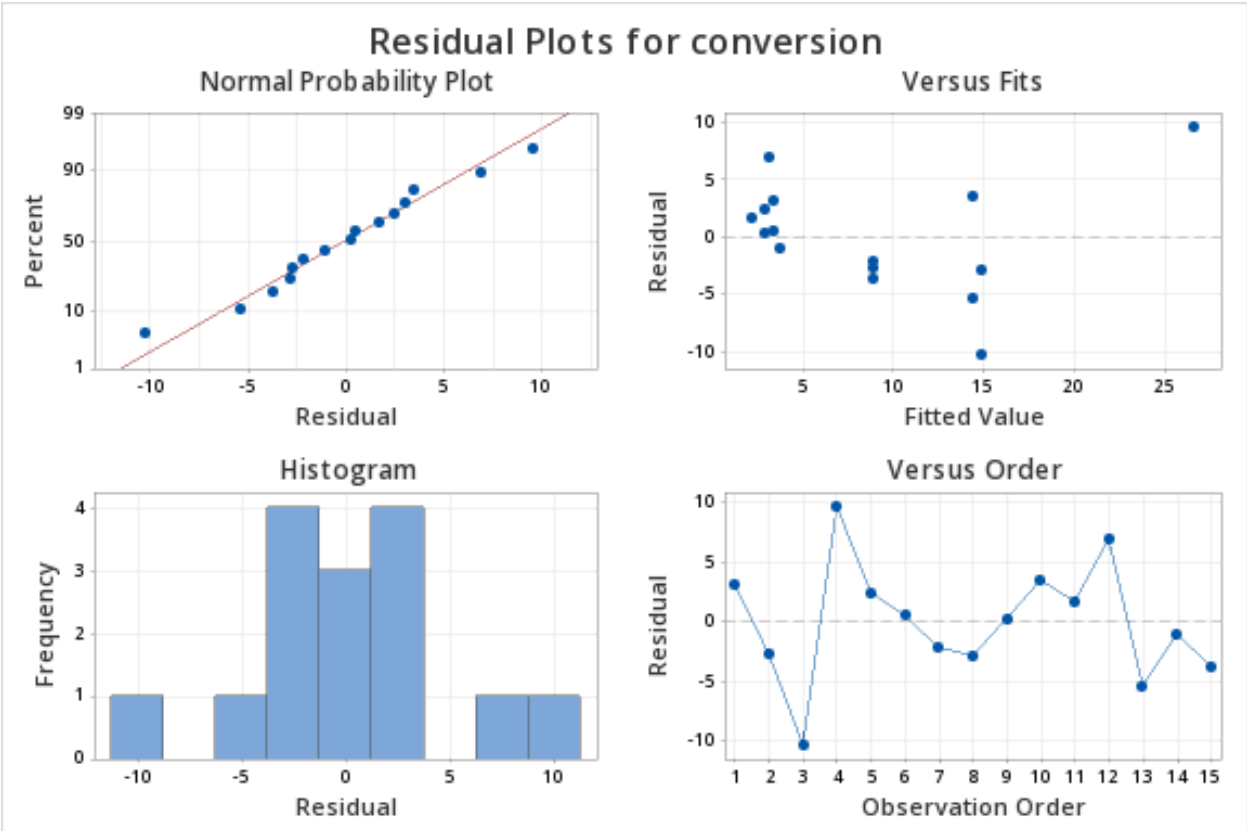
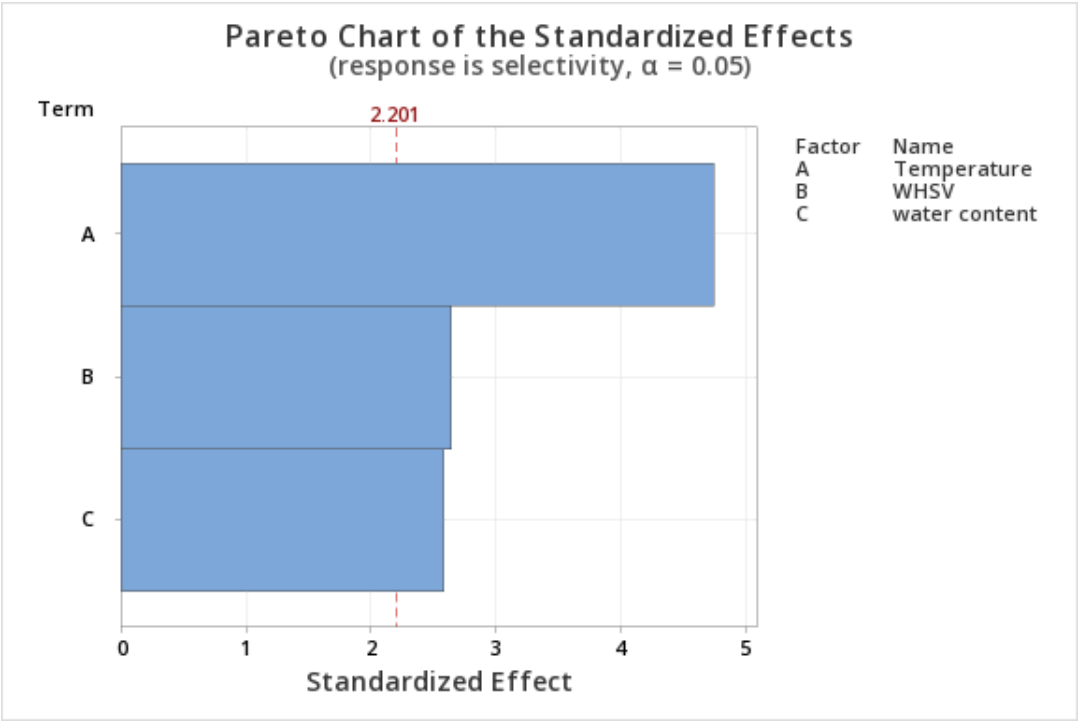
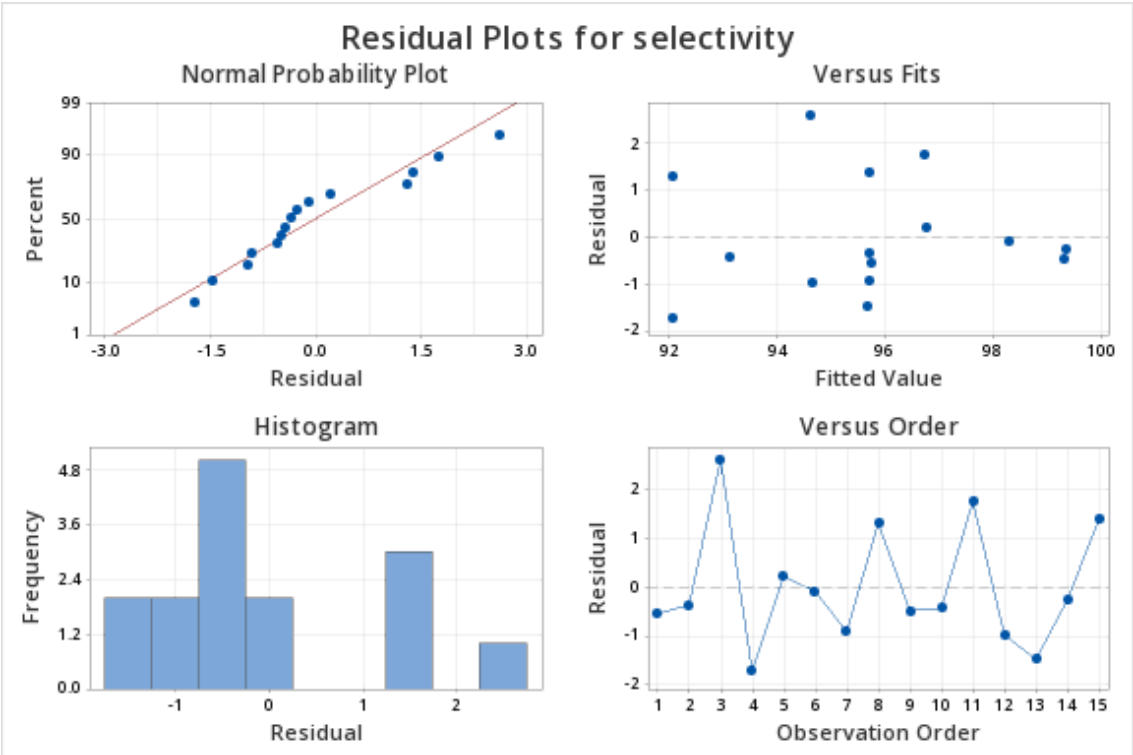


Figure S17. Residual plots of Box-Behnken model for conversion



**Figure S18.** Pareto chart Box-Behnken model for BD selectivity



**Figure S19.** Residual plots of Box-Behnken model for selectivity

**Table S1.** Summary of results for dehydra-decyclization of THF over P-MFI.

Run #	Temperature (°C)	WHS V (h <sup>-1</sup> )	Water content in feed (%)	Conversion (%)	Selectivity (%)				Carbon balance (%)
					1,3-BD	Propene	Butenes	Others <sup>1</sup>	
1	200	1.9	0	5.8	95.0	0.9	3.1	1.0	99.9
2	250	1.9	0	8.7	94.0	1.1	3.4	1.5	99.8
3	300	1.9	0	21.5	94.1	1.4	2.8	1.8	99.5
4	350	1.9	0	39.8	92.7	2.7	2.5	2.1	99.8
5	360	1.9	0	44.3	90.5	3.9	2.3	3.3	98.1
6	370	1.9	0	50.2	89.4	5.2	1.7	3.8	97.4
7	200	10.5	0	4.9	97.0	1.0	1.3	0.7	99.9
8	250	10.5	0	6.9	92.9	1.8	4.2	1.1	99.9
9	300	10.5	0	13.5	94.2	2.1	2.5	1.2	99.8
10	350	10.5	0	15.9	94.4	2.3	2.1	1.2	99.7
11	360	10.5	0	16.4	93.9	2.9	1.5	1.7	99.6
12	370	10.5	0	16.7	93.4	3.2	1.1	2.3	99.5
13	285	10.5	5	6.2	95.4	1.7	2.1	0.8	99.9
14	370	1.9	5	36.3	90.4	3.8	2.3	3.3	98.5
15	285	1.9	10	9.1	94.2	1.3	3.0	1.5	99.8

<sup>1</sup> Predominantly unidentified large compounds.

**Table S2.** Summary of results for dehydra-decyclization of THF over Na P-MFI.

Run #	Temperature (°C)	WHS V (h <sup>-1</sup> )	Water content in feed (%)	Conversion (%)	Selectivity (%)			
					1,3_BD	Propene	Butenes	Others <sup>1</sup>
1	360	1.0	0	41.9	85.0	2.5	5.0	7.5
2	360	1.9	0	40.8	88.5	3.5	2.0	6.0
3	360	10.5	0	7.2	96.5	1.0	0.5	2.0
4	360	19.1	0	6.2	97.4	1.0	0.6	1.0
5	300	10.5	0	4.8	87.5	5.5	0.0	7.0
6	360	10.5	10	14.9	93.0	2.5	1.5	3.0
7	370	10.5	0	11.1	98.5	0.4	0.1	1.0
8	300	1.9	0	25.3	90.5	3.5	1.5	4.5
9	360	19.1	10	6.2	97.4	0.9	0.2	1.5

<sup>1</sup> Predominantly unidentified large compounds.

**Table S3.** Summary of results for dehydra-decyclization of THF over B-MFI.

Run #	Temperature (°C)	WHS V (h <sup>-1</sup> )	Water content in feed (%)	Conversion (%)	Selectivity (%)			
					1,3_BD	Propene	Butenes	Others <sup>1</sup>
1	200	1.9	0	2.9	75.0	2.0	15.0	8.0
2	250	1.9	0	4.5	72.0	2.4	14	11.6
3	350	1.9	0	20.8	68.0	5.0	12.0	15.0
4	370	1.9	0	31.3	63.4	9.8	11.8	15.0
5	400	1.9	0	36.0	60.0	10.2	11.2	18.6
6	200	0.19	0	11.1	70.0	3.0	9.0	18.0
7	370	0.19	0	53.3	61.0	7.0	12.0	20.0
8	370	0.38	40	19.9	74.0	5.5	8.0	12.5
9	200	10.5	0	1.3	73.0	4.0	7.0	16.0
10	370	10.5	0	7.9	65.0	8.0	12.0	15.0
11	285	1.9	0	8.1	69.0	5.0	9.0	17.0
12	370	19.1	0	6.4	64.5	6.7	10.2	18.6
13	350	1	0	39.8	67.0	4.5	12.0	16.5
14	370	1	5	20.0	75.0	5.4	11.0	8.6
15	370	1	10	7.2	74.0	5.6	9.0	11.4
16	200	1	10	7.6	77.0	3.0	8.7	11.3

<sup>1</sup> Predominantly unidentified large compounds.

**Table S4.** Summary of results for dehydra-decyclization of THF over S-MFI.

Run #	Temperature (°C)	WHS V (h <sup>-1</sup> )	Water content in feed (%)	Conversion (%)	Selectivity (%)			
					1,3_BD	Propene	Butenes	Others <sup>1</sup>
1	350	1	10	5.4	92.0	2.5	1.4	4.1
2	360	1.9	0	19.8	95.7	1.2	0.8	2.3
3	200	10.5	0	1.4	97.0	0.6	1.1	1.3
4	285	1.9	0	6.5	96.5	0.3	1.1	2.1
5	370	19.1	0	8.6	91	0.9	1.4	6.7
6	285	19.1	0	3.0	97.0	0.2	0.7	2.1
7	370	10.5	0	10.8	91.0	1.7	0.7	6.6
8	285	10.5	5	6.7	98.0	0.2	0.7	1.1
9	370	10.5	5	10.8	92.5	1.6	1.2	4.7
10	370	19.1	10	6.9	92.5	1.5	0.9	5.1
11	350	1	0	30.3	88.5	1.8	2.2	7.5
12	350	1	5	28.9	90.5	1.3	1.7	6.5
13	350	1	10	12.0	92.7	0.8	1.2	5.3
14	370	1	10	15.3	91.2	1.2	1.7	5.9
15	300	1	10	6.5	94.5	0.6	0.9	4
<sup>1</sup> Predominantly unidentified large compounds.								

**Table S5.** Property summary of the analysis of variance through Box-Behnken for THF conversion and 1,3-BD selectivity response surface models for P-MFI.

Source	Degrees of freedom (DF)	T-value	F-value	P-value <sup>a</sup>	R <sup>2</sup> (%)	R <sup>2</sup> (adjusted) (%)	R <sup>2</sup> (predicted) (%)
Conversion model	3		7.4	0.006	66.9	57.8	0.0
Constant		6.2					
Temperature	1	3.1	9.3	0.011			
WHSV	1	-2.8	7.8	0.017			
Temperature*WHSV	1	-2.3	5.1	0.046			
Error	11						
Lack of fit	9		62.7	0.016			
Pure error	2						
Selectivity model	3						
Constant	-	266.1	12.1	0.001	76.8	70.4	53.4
Temperature	1	-4.8	22.6	0.001			
WHSV	1	2.7	7.0	0.023			
Water content	1	2.6	6.7	0.025			
Error	11						
Lack of fit	9		1.4	0.479			
Pure error	2						

<sup>a</sup>  $\alpha = 0.05$

**Table S6.** Distance ( $r$ ) in Å of the O atom and the acid site (H1, H2, or Hzeo). Relative interaction energies ( $\Delta E_{IE}$ ) of THF with acid sites. THF electron affinity energies ( $\Delta E_{EA}$ ). The deprotonation was computed by elongating its distance until it reached the oxygen atom in THF. The H1 site corresponds to the acidic proton closest to the surface proton, Hzeo. Energies are in kcal/mol and computed at the M06-2X/def2-SVP:AM1 level.

	H1			H2			Hzeo		
	$r$	$\Delta E_{IE}$	$\Delta E_{EA}$	$r$	$\Delta E_{IE}$	$\Delta E_{EA}$	$r$	$\Delta E_{IE}$	$\Delta E_{EA}$
B-MFI	0.977	0.0	59.1	0.984	-5.4	65.3	0.985	3.3	63.2
P-MFI	1.031	0.0	45.8	1.011	4.9	52.0	0.987	0.6	56.6
S-MFI	0.986	0.0	28.0	NA	NA	NA	0.969	-1.8	59.0

**Table S7.** Relative energies (kcal/mol) of the dehydra-decyclization of THF on ZSM5 functionalized with aluminum, boric, phosphoric, and sulfuric acid.

	Aluminum	Boron	Phosphorus	Sulfur
<b>1</b>	0.0	0.0	0.0	0.0
<b>2</b>	-23.0	-14.5 (-9.1)	-12.6 (-7.7)	-14.1
<b>2-Hzeolite</b>	NA	-11.2	-7.1	-15.4
<b>3</b>	-8.8	-1.7	-0.9	-0.3
Retro-Prins	12.5	20.5	24.9	20.1
<b>4</b>	-20.5	0.2	1.2	-21.3
<b>5</b>	-15.5	-5.3	4.2	-4.9
<b>6</b>	-0.7	8.6	16.7	<b>6.2 (20.4<sup>A</sup>)</b>

<sup>A</sup>The value of the deprotonation energy in the absence of water

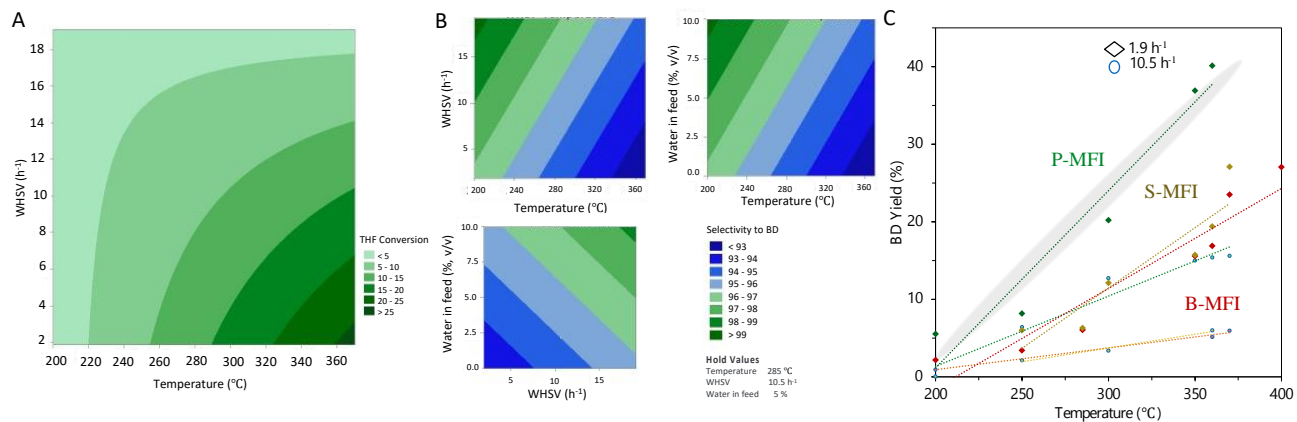
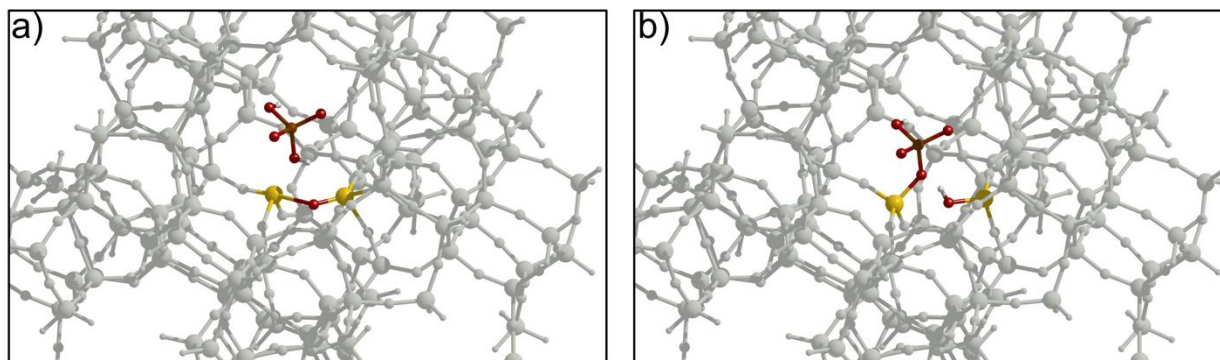


**Figure S20.** Modeled contour plots depicting the pair-interaction effect of process variables on A THF conversion and B selectivity to 1,3-BD for P-MFI for  $\alpha = 0.05$ . C displays 1,3-BD yield for 100 % THF theoretical conversion, diamonds with a darker shade represent values at  $1.9 \text{ h}^{-1}$  and circles with a lighter shade the values at  $10.5 \text{ h}^{-1}$ . The trendlines are added as a visual guide.



**Scheme S2.** Representation of the coordination of the acid ( $\text{H}_2\text{SO}_4$ ) into the zeolite. (a) the acid approaches the T12 site. (b) the acid cleaves one Si-O bond, and the resulting deprotonated O on the acid binds to the Si atom, and the proton coordinates to the adjacent surface O atom, forming a BAS.

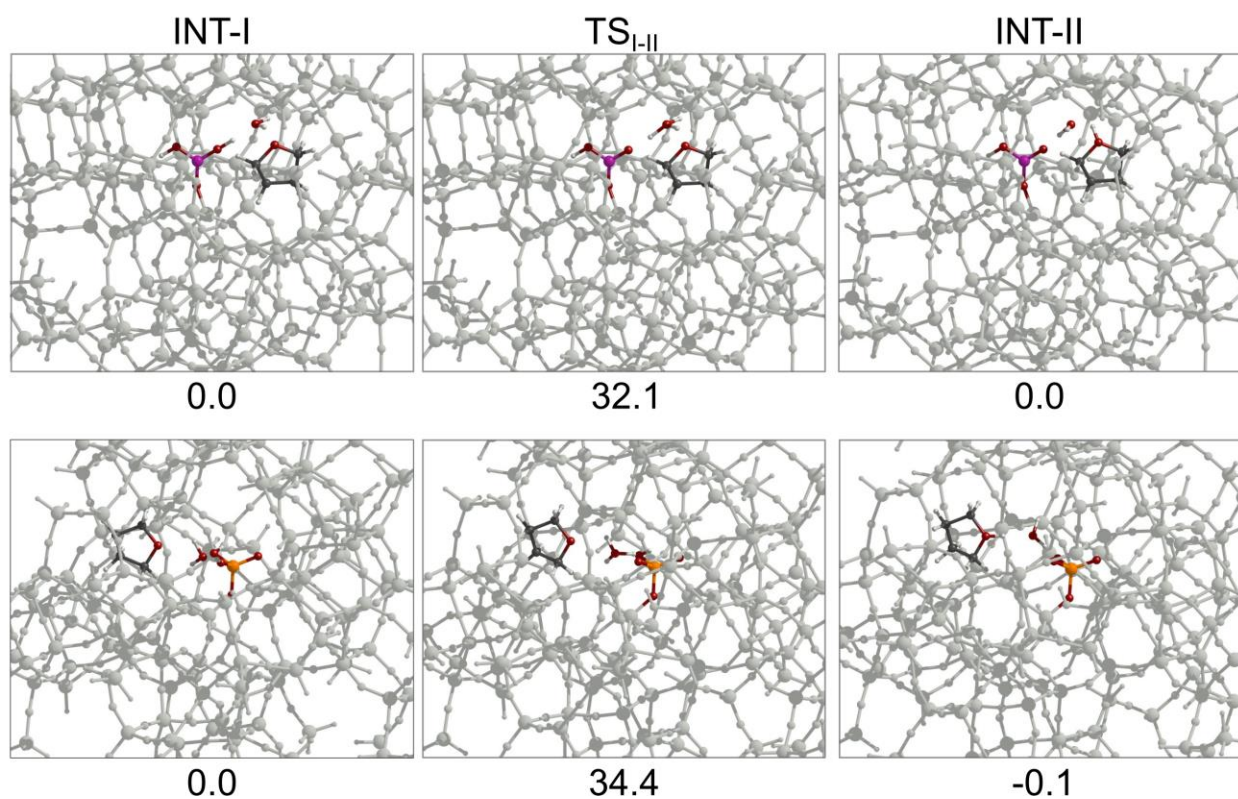


**Figure S21.** Tetrahydrofuran protonation steps from intermediate INT-I to intermediate INT-II through transition state TS<sub>I-II</sub> involving an explicit water molecule for B-MFI (top panel) and P-MFI (bottom panel). Energies in kcal/mol computed at the M06-2X/def2-SVP:AM1 level.

## Active site coordination

Various articles stress that it is imperative to elucidate the chemical properties of diene selective phosphorus zeolites [1]–[3], and consequently elucidate the characteristics of similar (1,3-BD selective) catalysts, such as S-MFI, first tested in this work. By studying the chemical state of the active groups (Figure S17) we hope to shed light into in-situ active site evolutive pathway and deepen our understanding of the thermochemical mechanistic.

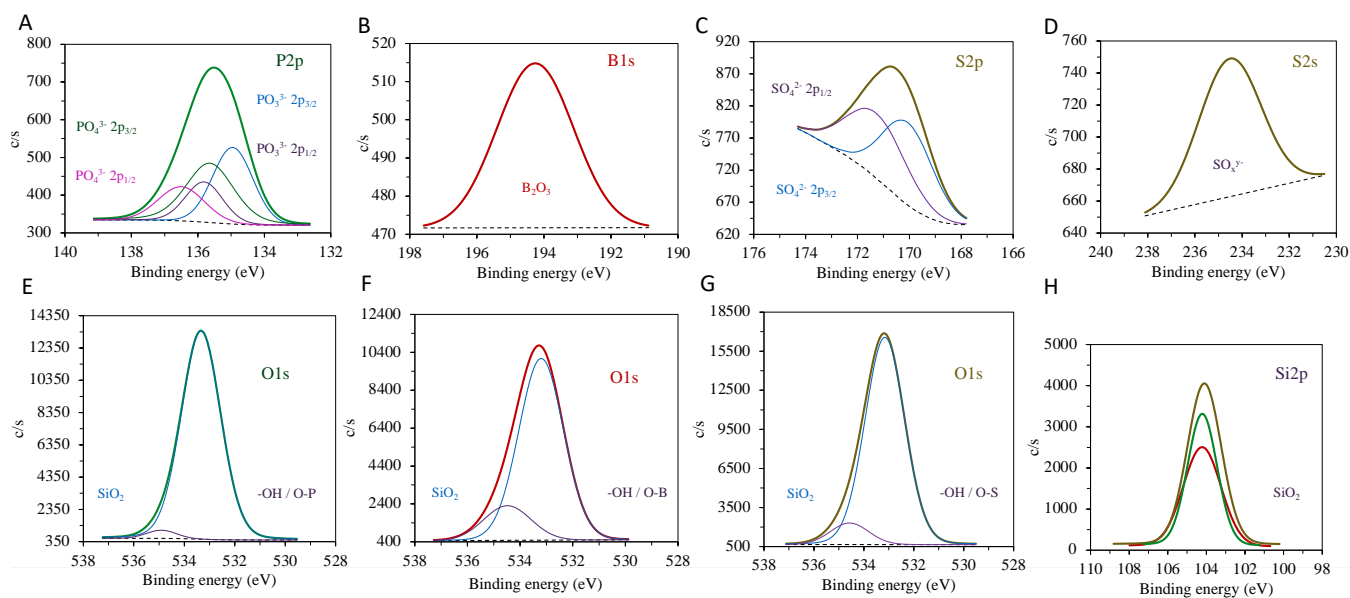


**Figure S22.** Analysis of active site chemical state in P-MFI, B-MFI, and S-MFI with XPS surface technique.

Ruiz-Zamora and co-workers have recently confirmed the active sites in P-SPP catalysts to have the form of orthophosphate groups [4]. Our analyses confirm the presence of phosphate ( $\text{PO}_4^{3-}$ ) and phosphite ( $\text{PO}_3^{3-}$ ) groups in the P-MFI catalyst (Figure S22A). The  $\text{PO}_4^{3-}$ , and  $\text{PO}_3^{3-}$  peaks have been deconvoluted into their respective  $p_{1/2}$  and  $p_{2/3}$  peaks. In accordance with the science, the ratio of  $p_{1/2}$  and  $p_{2/3}$  peaks is  $\sim 1/2$ . Both  $\text{PO}_4^{3-}$ , and  $\text{PO}_3^{3-}$  groups occur in proportionate amounts. BAS activity can be associated with  $\text{PO}_4^{3-}$  groups [3], [5]. However, the lone pairs in  $\text{PO}_3^{3-}$  could evolve into complex and oligomeric active centers, opening the possibility of initiating the conversion of THF via a BAS, affected by other interactions such as hydrogen bonding, and / or ionic pairings [6]. This could support why the conversion model (Table S5) could not be effectively concerted based solely on BAS pathways. The trigonal coordination of boron in borosilicates has also been confirmed (Figure S22B), as such, the reported hydration mechanism (Scheme 2) can be considered representative of the active site evolutive pathway. Sulphate ( $\text{SO}_4^{2-}$ ) groups have been identified as the primary active center in S-MFI. Furthermore, these groups can have variable nature ( $\text{SO}_x^{y-}$ ) and BAS counts, which will depend for instance on the temperature and humidity the catalyst is exposed to. Interestingly, the proportion of  $\text{SiO}_2$  groups decrease in the catalysts in the order of S-MFI > P-MFI > B-MFI (Figure S22H), in agreement with selectivity to 1,3-BD values (Figure 1). This indeed implies that  $\text{SiO}_2$  network (and the presence of defects thereof) is an important factor determining shape-selectivity to 1,3-BD [3]. Moreover, the proportion of O-X groups (Figure S22 E-G) also agrees with conversion trends (Figure 1), P-MFI with the smallest O-X peak (Figure S22E)  $\sim 1059$  c/s, had the highest conversion, while the B-MFI and S-MFI O-X peaks (Figure S22 F and G) are comparable,  $\sim 2305$  c/s and  $\sim 2308$  c/s respectively, and the

catalysts displayed statistically similar levels of conversion based on Tukey's pairwise comparison of means. These values could be used to design and prognosticate the performance of innovative zeosil catalysts prior to running experimental tests.

### Temperature effect on active site evolution

The infrared spectra of P-MFI, B-MFI, S-MFI, and THF doped S-MFI are shown in Figure S18. The skeletal structures are uniform, and in accordance with reported MFI FTIR spectra [7].

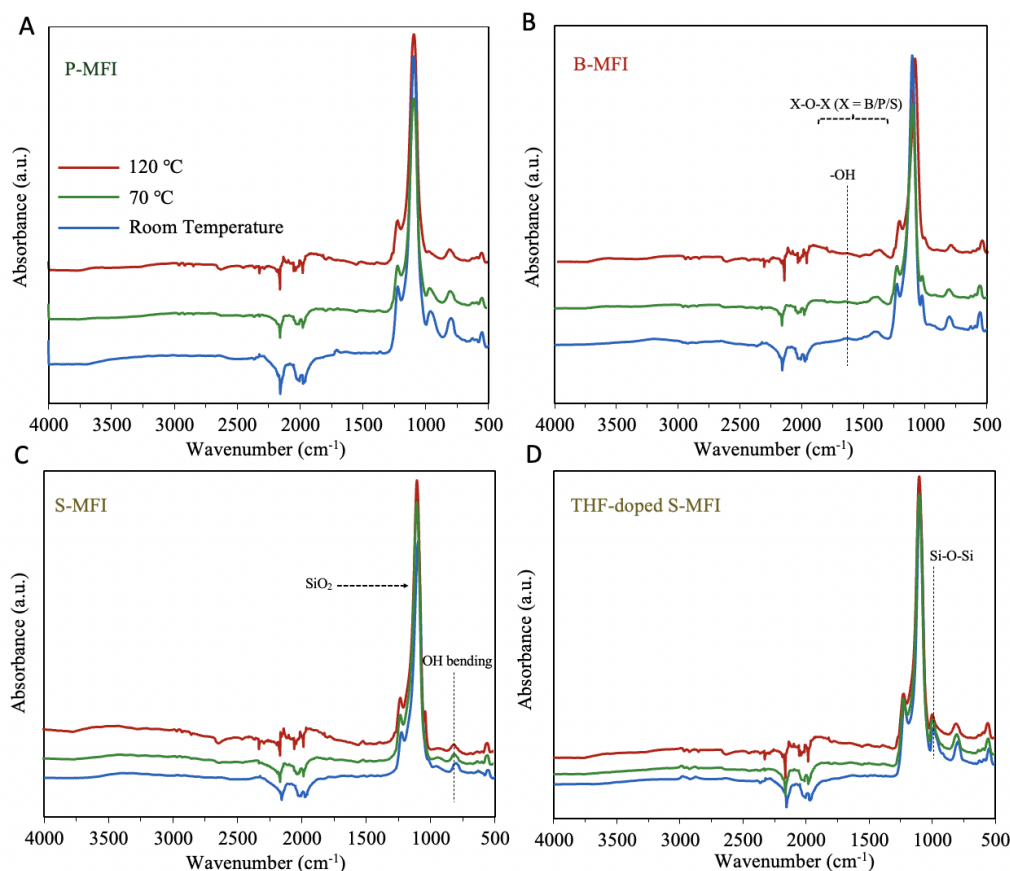


**Figure S23.** Infrared spectra as a function of temperature, room temperature, 70 °C, and 120 °C for **A** P-MFI **B** B-MFI **C** S-MFI, **D** THF-doped S-MFI. The spectra are ATR corrected.

The SiO<sub>2</sub> band at about 1100 cm<sup>-1</sup> appears well defined in all the samples (Figure S23), yet more pronounced at higher temperatures for P-MFI, and S-MFI. This implies re-link of silanol nests into the framework, as previously suggested, and framework regeneration would improve selectivity to 1,3-BD. Whereas in B-MFI this peak was constant with temperature, implying irreversible defects in the borosilicates that decrease selectivity to 1,3-BD [8]. The external tetrahedra Si-O-Si band at ~ 980 cm<sup>-1</sup> is minute in B-MFI and S-MFI suggesting that these have been replaced for Si-O-X linkages. Furthermore, the decreased intensity with temperature in P-MFI implies that the phosphorus active sites evolve as a function of temperature, confirming what was hypothesized before in Table S5. Additionally, the Si-O-Si band is more pronounced in the THF-doped S-MFI sample, and considering Figure S22 C and D sequentially, in-situ steaming resulting from THF dehydro-decyclization could be evolving the sulfur active site as proposed in Scheme 2.

## References

- [1] S. Li *et al.*, “Dehydra-Decyclization of Tetrahydrofuran on H $\beta$ -ZSM5: Mechanisms, Pathways, and Transition State Entropy,” *ACS Catal.*, vol. 9, no. 11, pp. 10279–10293, 2019, doi: 10.1021/acscatal.9b03129.
- [2] O. A. Abdelrahman *et al.*, “Biomass-Derived Butadiene by Dehydra-Decyclization of Tetrahydrofuran,” *ACS Sustain. Chem. Eng.*, vol. 5, no. 5, pp. 3732–3736, 2017, doi: 10.1021/acssuschemeng.7b00745.
- [3] S. K. Jain *et al.*, “P-site structural diversity and evolution in a zeosil catalyst,” *J. Am. Chem. Soc.*, vol. 143, no. 4, pp. 1968–1983, Feb. 2021, doi: 10.1021/jacs.0c11768.
- [4] E. Ruiz-Zamora *et al.*, “Siliceous self-pillared pentasil (SPP) zeolite with incorporated phosphorus groups in catalytic formation of butadiene by dehydra-decyclization of tetrahydrofuran: Study of catalyst stability by NMR and REDOR analysis,” *Appl. Catal. A. Gen.*, vol. 640, 2022, doi: 10.1016/j.apcata.2022.118648.
- [5] N. C. Nelson, Z. Wang, P. Naik, J. S. Manzano, M. Pruski, and I. I. Slowing, “Phosphate modified ceria as a Brønsted acidic/redox multifunctional catalyst,” *J. Mater. Chem. A. Mater. Energy Sustain.*, vol. 5, no. 9, pp. 4455–4466, 2017, doi: 10.1039/C6TA08703E.
- [6] D. Parmar, E. Sugiono, S. Raja, and M. Rueping, “Complete Field Guide to Asymmetric BINOL-Phosphate Derived Brønsted Acid and Metal Catalysis: History and Classification by Mode of Activation,” *Chem. Rev.*, vol. 114, no. 18, pp. 9047–9153, 2014, doi: 10.1021/cr5001496.
- [7] A. Kessouri, B. Boukoussa, A. Bengueddach, and R. Hamacha, “Synthesis of iron-MFI zeolite and its photocatalytic application for hydroxylation of phenol,” *Res. Chem. Intermed.*, vol. 44, no. 4, pp. 2475–2487, 2017, doi: 10.1007/s11164-017-3241-8.
- [8] G. Kumar, D. Liu, D. Xu, L. Ren, M. Tsapatsis, and P. J. Dauenhauer, “Dehydra-decyclization of 2-methyltetrahydrofuran to pentadienes on boron-containing zeolites,” *Green Chem.*, vol. 22, no. 13, pp. 4147–4160, 2020, doi: 10.1039/d0gc00136h.